

In the present report we have tried to be as quantitative as possible for two-layer materials. The pairing mechanism within a given layer was assumed to be BCS-type electron-phonon interaction because we believe this to be the most realistic possibility. In previous work (1, 15) we gave a simple formula for  $T_j$  which can be used to generalize to other materials with variable layer numbers (including single-layer compounds for which  $T_j$  characterizes the coupling between the CuO layers in adjacent unit cells), and have shown that it yields a good heuristic fit to  $T_c$  versus number of layers for Bi and Tl one-, two-, and three-layer materials as well as a prediction for  $\infty$ -layer materials. This leads to a near zero  $T_c$  for Bi one-layer materials, but to a  $T_c \sim 60$  to 70 K for Tl one-layer materials [ $T_j$  is considerably larger in this case (16)]. The fit to the recently discovered Hg-based materials (17) is also satisfactory. A prediction, based on the present ideas, is that  $\text{La}_{2-x}\text{Sr}_x\text{CuO}_4$  as well as  $\text{Nd}_{2-x}\text{Ce}_x\text{CuO}_4$  should exhibit roughly isotropic gaps because  $t_{\perp}(\mathbf{k})$  is not very anisotropic within tight-binding approximation.

## REFERENCES AND NOTES

1. P. W. Anderson, in *Superconductivity, Proceedings of the ICTP Spring College in 1992*, P. Butcher and Y. Lu, Eds. (World Scientific, Singapore, in press).
2. Z.-X. Shen *et al.*, *Phys. Rev. Lett.* **70**, 1553 (1993).
3. V. J. Emery, *Ann. Phys. N.Y.* **28**, 1 (1964).
4. P. W. Anderson, *Science* **256**, 1526 (1992); C. M. Varma *et al.*, *Phys. Rev. Lett.* **63**, 1996 (1989); *ibid.* **64**, 497 (1990), erratum.
5. G. D. Mahan, *Many Particle Physics* (Plenum, New York, 1990). For a recent discussion of the orthogonality catastrophe, see P. W. Anderson (*Math. Rev.*, in press) and references therein. If we adiabatically decouple the motion of an electron perpendicular to the layers, for each  $\mathbf{k}$ , one can construct a two-state system coupled to the bath of in-plane excitations. In a non-Fermi liquid any attempt to tunnel between the layers will significantly disturb all the electrons in the system. Thus, the tunneling matrix element will be multiplied by a overlap matrix element involving  $N(N \rightarrow \infty)$  electrons, which can vanish depending on the spectral density of the bath of excitations; see S. Chakravarty, *Phys. Rev. Lett.* **49**, 681 (1982), and A. J. Leggett *et al.*, *Rev. Mod. Phys.* **59**, 1 (1987). Here, this would happen if the spectral function corresponding to the one-particle Green's function satisfies the homogeneity relation  $A(\Lambda\omega, \Lambda k) = \Lambda^{\alpha-1} A(\omega, k)$  and the exponent  $\alpha \geq 1$ . There are, however, logarithmic corrections as  $\alpha \rightarrow 1$ . The value  $\alpha = 1$  will lead to a precise linear  $T$  dependence of the in-plane resistivity in these materials. We emphasize that the physical effect will not be very different even if  $\alpha < 1$  provided that  $T$  is larger than the crossover temperature  $t_{\perp}(t_{\perp}/W)^{\alpha/(1-\alpha)}$ , where  $W$  is of the order of the bandwidth. For another derivation, see P. W. Anderson, in preparation.
6. See, for example, B. Batlogg in *High Temperature Superconductivity*, K. S. Bedell *et al.*, Eds. (Addison-Wesley, Redding, MA, 1990). The observation, in some samples, of a  $c$ -axis resistivity which follows a linear (or more complex) temperature dependence does not imply coherent tunneling of quasiparticles between the planes. This behavior can arise if the hopping rate between the layers, renormalized by the coupling to the intralayer excitations, is smaller than the temperature; a crucial point is that the magnitude of the  $c$ -axis resistivity seems to be considerably larger than the  $ab$  plane resistivity, generally much above the Mott limit at  $T_c$ ; see N. Kumar and A. M. Jayanavar, *Phys. Rev. B* **45**, 5001 (1992).
7. That  $\mathbf{k}_F$  remains unshifted in the Luttinger model was first pointed out by D. C. Mattis and E. H. Lieb, *J. Math. Phys.* **6**, 304 (1965). This follows from a counting argument because there are no level crossings. Such a counting argument is independent of the dimensionality of the electron gas.
8. C. G. Olson *et al.*, *Science* **245**, 731 (1989); D. S. Dessau *et al.*, *Phys. Rev. Lett.* **66**, 2160 (1991).
9. K. Tamasaku, Y. Nakamura, S. Uchida, *Phys. Rev. Lett.* **69**, 1455 (1992).
10. See, for example, J. Yu and A. J. Freeman, *J. Phys. Chem. Solids* **52**, 1351 (1991).
11. See, for example, S. Massida, J. Yu, A. J. Freeman, *Physica C* **152**, 251 (1988); M. S. Hybertsen and L. F. Mattheiss, *Phys. Rev. Lett.* **60**, 1661 (1988); H. Krakauer and W. E. Pickett, *ibid.*, p. 1665.
12. P. W. Anderson, *Phys. Rev.* **112**, 1900 (1958).
13. J. Tranquada *et al.*, *Phys. Rev. B* **40**, 4503 (1989); J. Tranquada *et al.*, *ibid.* **46**, 5561 (1992). Note that for  $O_{6g}$ , the optic mode in the spin wave spectrum due to bilayers was not observed up to 60 meV. For  $O_{6g}$ , some indication of the optic mode has been observed for energies greater than 40 meV.
14. D. A. Bonn *et al.*, *Phys. Rev. Lett.* **68**, 2390 (1991).
15. J. M. Wheatley, T. C. Hsu, P. W. Anderson, *Phys. Rev. B* **37**, 5897 (1988).
16. We argue this on the basis of the band structure calculations of D. J. Singh and W. E. Pickett [*Physica C* **203**, 193 (1992)] and D. R. Hamann and L. F. Mattheiss [*Phys. Rev. B* **38**, 5138 (1988)].
17. A. Schilling *et al.*, *Nature* **363**, 56 (1993); S. N. Putilin *et al.*, *ibid.* **362**, 226 (1993).
18. We thank E. Abrahams, W. E. Pickett, and Z.-X. Shen for useful discussions. This work was supported in part by the National Science Foundation, DMR-9104873 (P.W.A. and S.S.), DMR-9220416 (S.C.), and in part by the Office of Naval Research, ONR-92J1101 (S.C. and A.S.). S.C. also thanks the John Simon Guggenheim Memorial Foundation for support through a fellowship and S.S. the AT&T Bell Laboratories for a Ph.D. scholarship.

2 April 1993; accepted 28 May 1993

## How Fish Power Swimming

Lawrence C. Rome,\* Douglas Swank, David Corda

It is thought that fish generate the power needed for steady swimming with their anterior musculature, whereas the posterior musculature only transmits forces to the tail and does negative work. Isolated red muscle bundles driven through the length changes and stimulation pattern that muscles normally undergo during steady swimming showed the opposite pattern. Most of the power for swimming came from muscle in the posterior region of the fish, and relatively little came from the anterior musculature. In addition, the contractile properties of the muscle along the length of the fish are significantly adapted to enhance power generation.

To maintain a constant velocity through a viscous medium, a body must generate mechanical power. In fish, the mechanical power is generated by muscle. It is thought that during typical swimming (caudal fin propulsion), most of the power is exerted on the water by the tail (1). Therefore, the power must either be generated by the musculature adjacent to the tail or be somehow transmitted to the tail. A combination of kinematics, electromyography, and mathematical modeling led to the current theory that there is a systematic shift in muscle function along the length of the fish. Specifically, the anterior musculature generates most of the power (by shortening contractions, which produce positive work), and the posterior musculature only transmits force to the tail [by lengthening

contractions, in which the muscle develops tension but is lengthened rather than shortened; this greatly stiffens the muscle (2) but produces negative work (3)]. Thus, by analogy (4), the anterior muscle is the "motor," the tail is the "propeller," and the lengthening posterior muscle is the "drive shaft." Although this hypothesis is widely accepted, it has never been rigorously tested.

We therefore measured the power that was generated by muscle at various places along the length of the fish. Power generated by muscle is the product of tailbeat frequency and the work per tailbeat (that is,  $Fd\ell$ , where  $F$  is force and  $\ell$  is length, integrated over the tailbeat cycle). Thus, in theory, one need only measure the instantaneous force production and length change of the muscle during the tailbeat cycle to determine power production at a particular position on the fish. Although muscle length changes can be measured during swimming, it is not experimentally possible to measure force production directly (fish musculature precludes the use of an in vivo force transducer). However, because the force produced by muscle is a function of

L. C. Rome and D. Corda, Department of Biology, University of Pennsylvania, Philadelphia, PA 19104, Coastal Research Center, Woods Hole Oceanographic Institution, and Marine Biological Laboratories, Woods Hole, MA 02543.  
D. Swank, Department of Physiology, University of Pennsylvania, Philadelphia, PA 19104.

\*To whom correspondence should be addressed.

the length change and the stimulation pattern it undergoes (5, 6), we determined this force experimentally by driving isolated muscle through the exact length changes and stimulation pattern it undergoes in a swimming fish and then measuring the resulting force.

To make these measurements, we studied scup (*Stenotomus chrysops*) swimming steadily at 80 cm/s, their maximum speed while using red muscle fibers only. Studying red muscle had several advantages. First, the red fibers power most of the caudal fin swimming behavior in fish (7-9). Second, as opposed to the white muscle (which has a complex geometry), the red muscle fibers run parallel to the long axis of the fish, which simplifies the relation of muscle shortening to backbone curvature [determined from films (10, 11)]. Finally, as

opposed to the erratic "burst and coast swimming" associated with use of white muscle (12), when using their red muscle, fish swim steadily and thus stay in a fixed position while swimming against a constant flow of water in a water treadmill (13, 14). This makes it possible to obtain the accurate films and electromyographs (EMGs) necessary for determination of the muscle length changes and stimulation pattern (15).

We filmed (200 frames per second) six scup in the treadmill from above and simultaneously recorded EMGs from the red musculature at four places along the length of the fish [labeled ANT-1, ANT-2, MID, and POST; 29, 40, 54, and 70%, respectively, of the distance from the nose to the tail (16)] (Fig. 1). Sarcomere length changes were determined from a combination of anatomical measurements and measure-

ments of backbone curvature from the films (10-12). The EMGs were synchronized to the sarcomere length changes to within  $\pm 0.2$  ms with a digital device (17, 18).

Moving caudally along the length of the fish, the length change of the muscle became larger. Strains were  $\pm 1.5\%$  of resting muscle length (resting sarcomere length was  $2.10 \mu\text{m}$ ) at ANT-1 and increased to  $\pm 5.7\%$  at POST (Fig. 1A). In addition, the EMGs had a longer duty cycle in the anterior of the fish than in the posterior (Table 1). This is caused primarily by a large difference in the onset time of the EMG in the anterior compared with the posterior but nearly simultaneous off times. Synchronization of EMGs with length changes showed that the EMG activity precedes the maximum length by increasing amounts along the length of the fish toward the tail (19) (Figs. 1 and 2 and Table 1).

To determine the mechanical performance of the muscle during this swimming behavior, we drove red muscle bundles isolated from the four positions on the fish

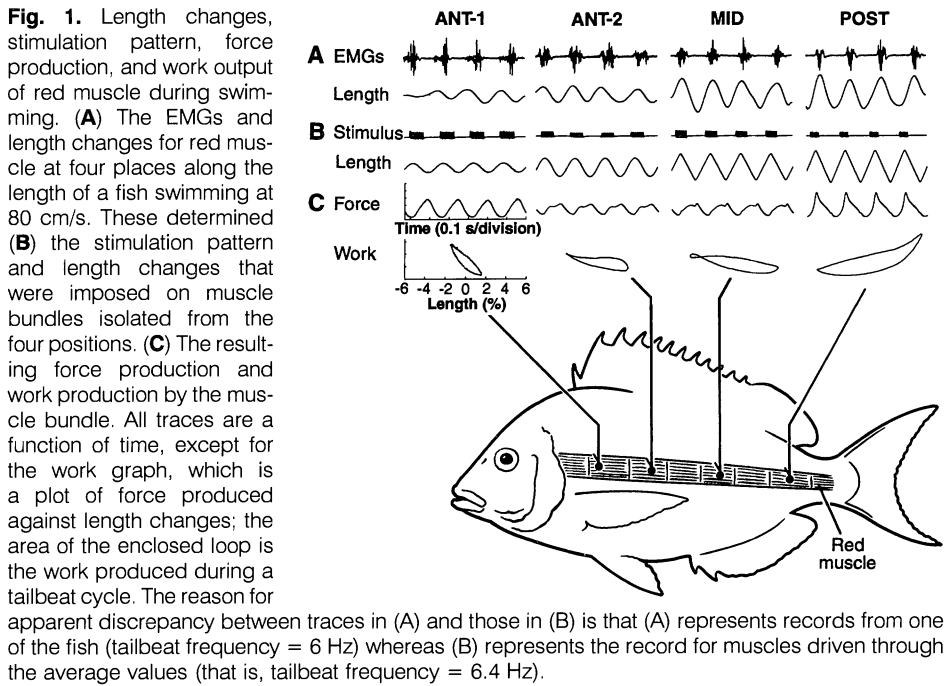


**Table 1.** Muscle parameters from swimming and isolated muscle experiments. Strain is the proportional length change of the muscle centered around the rest length. Duty cycle of EMG is the proportion of tailbeat cycle time that the muscle receives stimulation. Phase of stimulus is how much the EMG precedes the longest muscle length (based on  $360^\circ$  for a full tailbeat cycle). Power is the rate of work the muscle produces as it is driven under the in vivo stimulus and length change pattern (tailbeat frequency was 6.4 Hz). Maximum power is the maximum the muscle is capable of generating (measured at 4.68 Hz). Percent of maximum power refers to the power the muscle generates while the fish swims at 80 cm/s. Relaxation time is the time taken for the force to drop from 90% to 10% of maximum force generated during an isometric tetanus. All are mean values with SE in parentheses.

| Position | Strain* (%)      | Duty cycle* (%) | Phase* (degrees) | Power† (W/kg) | Max. power† (W/kg) | % Max. power† | Relaxation time† (ms) |
|----------|------------------|-----------------|------------------|---------------|--------------------|---------------|-----------------------|
| ANT-1    | $\pm 1.6$ (0.17) | 45.7 (1.6)      | -32.5 (6.5)      | 4.39 (0.79)   | 38.46 (5.06)       | 11.3 (0.7)    | 131 (5.8)             |
| ANT-2    | $\pm 2.9$ (0.45) | 40.8 (1.6)      | -46.1 (2.03)     | 6.58 (0.63)   | 27.56 (1.21)       | 27.1 (3.3)    | 165 (18.7)            |
| MID      | $\pm 4.8$ (0.36) | 35.3 (2.2)      | -53.5 (4.29)     | 10.79 (0.60)  | 26.98 (4.37)       | 39.7 (4.8)    | 225 (17.4)            |
| POST     | $\pm 5.7$ (0.54) | 26.6 (1.2)      | -59.9 (4.95)     | 24.32 (4.33)  | 30.70 (5.40)       | 81.2 (1.9)    | 229 (22.7)            |

\*From  $n = 6$  experiments. †From  $n = 4$  to 5 experiments.

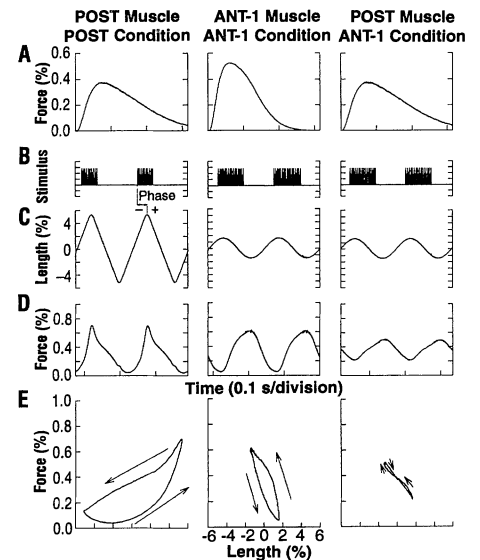


**Fig. 2.** Mechanical properties of ANT-1 and POST muscles. The first two columns show a POST and an ANT-1 muscle bundle undergoing their respective length changes and stimulation pattern that the muscle undergoes during swimming. In contrast, the third column shows a POST muscle driven with the stimulation pattern and length changes that are encountered by the ANT-1 muscle during swimming. (A) Isometric twitch of the muscles in question. The imposed (B) stimulation pattern and (C) length changes (the phase of the stimulus is defined with respect to maximum muscle length). (D) Resulting force and (E) work (area enclosed by loop), which is a plot of force as a function of length). Note that relaxation is much faster in muscle undergoing shortening (D) (caused by shortening deactivation) than that being held isometrically (A). All forces are in percent of maximum force generated during isometric tetanus.

through the length changes and stimulation conditions they undergo during swimming (20, 21) and measured the resulting force and power that the muscle generated (Fig. 1). Although the POST muscle is stimulated primarily during lengthening (Fig. 2), it generated large amounts of work (22). The anterior muscle, in contrast, generated significantly less work under its *in vivo* conditions (Figs. 1 and 2). Contrary to previous hypotheses, most of the power generated during this type of swimming is generated by the posterior musculature rather than the anterior musculature.

The cause of the low power generated in the anterior region of the fish was not an intrinsic deficiency of the anterior musculature; rather it was the specific length change and stimulation pattern of the anterior muscle. For instance, when the ANT-1 muscle is driven through the length change and stimulation pattern that the POST muscle normally undergoes *in vivo*, it generated as much power as the POST muscle (similar to Fig. 2, first column). The main reason for the low power output in the anterior region is the small strain ( $d\ell$ ) (23). A small  $d\ell$  reduces work output ( $Fd\ell$ ) per tailbeat. In addition, muscles undergoing small strains do not relax sufficiently fast. Relaxation is sped up greatly by muscle shortening (shortening deactivation), but the shorter the strain, the smaller this enhancement of relaxation (6, 24).

The ability of the ANT-1 muscle to produce any work at all during swimming represents an adaptation. When the POST muscle is driven through the length change and stimulation pattern that the ANT-1 muscle normally undergoes *in vivo*, it performed even worse than the ANT-1 muscle and generated no net work (Fig. 2, compare second and third columns). The primary reason that the ANT-1 muscle could generate significant power despite undergoing only a small strain (Fig. 2) is that it has a faster intrinsic relaxation rate than POST muscle (Fig. 2A and Table 1). Because of its slow intrinsic relaxation rate, POST muscle going through the ANT-1 conditions only partially relaxed between stimulus trains, whereas the ANT-1 muscle relaxed almost completely (Fig. 2D). The mechanism for faster relaxation in the ANT-1 muscle has yet to be explored.

Our conclusion that most of the power in swimming scup is generated by the middle and posterior musculature and relatively little is generated by the anterior musculature is further supported by additional kinematic analysis. When the tail is sweeping to one side and generating mechanical power (25), the posterior muscle on that side is shortening, not lengthening (lengthening of the posterior muscle during this period would be necessary for the previously pro-

posed hypothesis). The previous hypothesis was based on predictions of muscle performance made from length change and EMG records in the absence of isolated muscle experiments (22, 26).

The generation of power in the middle and posterior musculature seems to represent a superior design of the locomotory system because, in this case, all of the power generated by the musculature can be used to power swimming. In addition, the posterior muscle appears to be optimized for power generation because during these swimming movements, it shortens over the portions of the sarcomere length-tension and force-velocity curves where it generates maximum power (8). In the case of the alternative hypothesis, in which the posterior muscle would lengthen and perform negative work, a portion of the positive power generated by the anterior musculature would presumably be lost as heat in the posterior. Avoiding this loss may be essential in the case of the red muscle because it makes up less than 4% of the mass of the fish but powers all of steady swimming.

Thus, when the fish use their red muscle, forces are not transmitted to the tail by the lengthening of muscle in the posterior. If the fish were to use this strategy at all, it might be more useful for the white muscle (burst swimming). Anatomical measurements show that although the red muscle is fairly constant in absolute cross section, there is a large decrease in the cross section of the white muscle moving from the head to the tail. Therefore, when fish use their white muscle, they may have to transmit large forces from the large muscle cross section to the tail, and lengthening of posterior muscle while it is active might be one way to achieve this (27). This could be tested by the same procedures used here.

This experimental approach will have important future applications. It makes possible the accurate calculation of total mechanical power generated by the muscle during swimming (28), which may be useful for the evaluation of different hydrodynamic models of swimming as well as development of our understanding of how fish can locomote while expending far less energy than other animals (29). In addition, it will enable us to develop and test new ideas concerning how the muscular system is designed.

## REFERENCES AND NOTES

- M. J. Lighthill, *Proc. R. Soc. London Ser. B* **179**, 125 (1971).
- A. V. Hill [*ibid.* **126**, 136 (1938)] found that lengthening muscle generates much more force per cross-sectional area than shortening muscle.
- F. Hess and J. J. Videler, *J. Exp. Biol.* **109**, 229 (1984); J. L. van Leeuwen, M. J. M. Lankheet, H. A. Akster, J. W. M. Osse, *J. Zool.* **220**, 123 (1990).
- S. Wainwright [in *Fish Biomechanics*, P. W. Webb and D. Weihs, Eds. (Praeger, New York, 1983), chap. 3] developed this analogy but did not specify which element was the "drive shaft."
- R. K. Josephson, *J. Exp. Biol.* **114**, 493 (1985); J. D. Altringham and I. A. Johnston, *ibid.* **148**, 395 (1990); R. L. Marsh, J. M. Olson, S. K. Guzik, *Nature* **357**, 411 (1992).
- L. C. Rome and D. Swank, *J. Exp. Biol.* **171**, 261 (1992).
- L. C. Rome, P. T. Loughna, G. Goldspink, *Am. J. Physiol.* **247**, R272 (1984).
- L. C. Rome, I. Choi, G. Lutz, A. A. Sosnicki, *J. Exp. Biol.* **163**, 259 (1992); L. C. Rome, A. A. Sosnicki, I. Choi, *ibid.*, p. 281.
- The EMG electrodes that were placed in red and white muscle of carp and scup show that fish use only their red muscle at slow and moderate steady speeds and recruit white muscle at very high speeds. When they recruit white muscle, they fatigue rapidly and hence do not use this type of locomotion often (7, 8).
- L. C. Rome and A. A. Sosnicki, *Am. J. Physiol.* **260**, C289 (1990).
- In carp (7) and scup (8), the red muscle fibers run parallel to the long axis of the fish, and their sarcomere length changes can be modeled as a bending beam. We verified this by killing the fish, bending them, allowing the muscle to go into rigor, freezing them, and then measuring sarcomere length as a function of backbone curvature from frozen sections. White muscle is more complicated because the fibers run in a helical fashion.
- L. C. Rome, R. P. Funke, R. M. Alexander, *J. Exp. Biol.* **154**, 163 (1990).
- L. C. Rome *et al.*, *Nature* **355**, 824 (1988).
- The fish in this study swam in a Brett-type respirometer (8, 12, 13).
- With fish swimming in a fixed position with respect to the respirometer, they can be filmed at high magnification and short EMG electrodes can be used.
- The EMGs were recorded at 5 kHz with a computer system (DataPAC by Run Technology on a 486 personal computer). We also recorded EMGs from the white muscle to demonstrate that it is not active during steady swimming. The filming and basic EMG techniques were as described (8, 13).
- L. C. Rome, *J. Biomech.*, in press.
- In addition to being synchronized in time, the muscle length changes and EMGs were measured at precisely the same point on the fish. The EMG placement on each fish was determined with a stereotaxic device. We found the positions on each fish at which the length changes were determined with a computer program (10) and verified the result by filming fish with reflective markers attached to the positions usually occupied by the electrodes.
- The sarcomere length records were digitally filtered to remove high-frequency noise, which made the time of the maximum amplitude more clear for determination of phase of the stimulus. This was particularly necessary for the ANT-1 and ANT-2 positions, for which small strains made the signal-to-noise ratio low.
- This was accomplished with a computer-controlled servo and stimulator described elsewhere (6). The muscle was stimulated at an interpulse interval of ~5 ms (200 Hz) for the duration and phase found in the EMGs. A constant stimulation frequency is supported by quantitative EMG analysis (8). The interpulse interval was varied slightly ( $\pm 5\%$ ) between different conditions to provide the exact stimulation duration required.
- Spectral analysis of the length records from the MID and POST positions showed higher harmonics in addition to the fundamental frequency. Fitting with a ramp gave a better fit than a sine wave, and thus a rounded ramp (digitally smoothed at the corners) was used. The poor signal-to-noise ratio in the ANT-1 and ANT-2 positions made these spectra less distinct and quite variable. In this case, we used sinusoids to represent the muscle length changes because they are traditionally used. Additional mechanics experiments showed that the main conclusions from

- this study do not depend on which waveform was used.
22. It has been assumed that during the EMG burst, muscle is active and generates force but that the cessation of the EMG signal indicates that the muscle is no longer active or generating force. On the basis of this assumption, one would predict that the muscle undergoing the POST conditions would generate negative work because the muscle is lengthening for most of the time the EMG shows activity. However, the time taken for the muscle to activate and the long time taken for relaxation may greatly affect the mechanical performance (5). Hence, when the muscle is actually driven through this in vivo pattern, it generated nearly maximum positive power.
  23. In addition, not having the phase sufficiently negative also reduced the power output. Additional mechanics experiments showed that an increase in strain (from  $\pm 1.5$  to  $\pm 2.5\%$ ) or a shift in phase (back by  $15^\circ$ ) resulted in greater power production.
  24. R. K. Josephson, *J. Exp. Biol.* 147, 533 (1989); J. D. Altringham and I. A. Johnston, *ibid.* 151, 453 (1990).
  25. J. Tang and C. S. Wardle [*ibid.* 166, 33 (1992)] showed that most of the power is generated at the midpoint of the tail sweep in swimming salmon. D. Harper (personal communication) has obtained a similar finding in swimming scup. Superimposition of the tail-tip trace and muscle length change show that all the way back to the caudal peduncle, the muscle is shortening when the tail is sweeping to that side and generating power.
  26. Different species were used in this study than in (3). Although we have no reason to expect important species differences, they cannot be excluded without verification.
  27. The myosepta and skin have alternatively been proposed as transmission elements (4).
  28. The power developed by fish musculature has been approximated in the past from hydrodynamic calculations. These calculations, however, depend on a number of assumptions and the particular model used.
  29. K. Schmidt-Nielsen, *Science* 177, 222 (1972).

Although not having to support body weight would tend to reduce the energetic cost, having to move through a viscous media would tend to increase it. Accurate measures of muscle power will help evaluate the relative importance of the opposing effects.

30. We thank F. Carey and M. Grosenbaugh for advice on data analysis and organizing our stay at the Woods Hole Oceanographic Institution (WHOI); D. Leavitt, B. Lancaster, and B. Tripp for facilitating our work at the Coastal Research Center; M. Moore and B. Woodin for helping us find and maintain scup; D. Harper for advice on fish surgical techniques, for designing a surgical table, and for performing hydrodynamic calculations; R. Golder for illustrating the scup; L. Kerr for advice on image analysis; and F. Thurburg of the Bureau of Marine Fisheries for loaning us the water treadmill. This is WHOI contribution no. 8389. Supported by NIH AR38404 and NSF IBN 9205397.

4 March 1993; accepted 1 June 1993

## Formation of Magnetic Single-Domain Magnetite in Ocean Ridge Basalts with Implications for Sea-Floor Magnetism

Yen-Hong Shau,\* Donald R. Peacor, Eric J. Essene

Although magnetic data are the primary evidence for ocean floor spreading, the processes by which magnetic phases in ocean floor basalts are formed remain poorly constrained. Scanning transmission electron microscopic observations show that magnetic single-domain magnetite in sheeted dike basalts of Deep Sea Drilling Project hole 504B formed through oxidation-exsolution of ilmenite, exsolution of ulvöspinel lamellae, and recrystallization of end-member magnetite by interaction with convecting fluids. The data suggest that the sheeted dike basalts, with single-domain magnetite as an efficient and stable magnetic carrier, contribute significantly to sea-floor magnetism.

Paleomagnetic data from the oceanic crust constitute the primary evidence for sea-floor spreading at mid-ocean ridges (1-3). However, the nature and origin of the magnetic phases responsible for the sea-floor magnetism are not well understood. The primary Fe-Ti oxide mineral in mid-ocean ridge basalts is titanomagnetite, with an ~60 mole percent (mol %) ulvöspinel component ( $Usp_{60}$ ) and a Curie temperature of  $\sim 160^\circ\text{C}$  (4-6). However, magnetization data are generally not consistent with this phase. Rather, the observed magnetic properties (for example, an increase in Curie temperature and a decrease in remanence intensity) of the altered pillow basalts that occupy upper levels of the oceanic crust have been attributed to low-temperature oxidation or maghemitization (4-11). The results of studies of rock magnetism from Deep Sea Drilling Project (DSDP) hole 504B have shown that basalts

from the transition zone and from the sheeted dike complex generally have magnetic properties consistent with end-member magnetite as the magnetic carrier (6, 12, 13). Several mechanisms, such as oxidation-exsolution (14) or low-temperature maghemitization followed by phase inversion, have been proposed to account for the formation of magnetite that presumably exists on a submicroscopic scale (6, 12). Direct characterization of the magnetite with scanning transmission electron microscopy (STEM), scanning electron microscopy (SEM), and electron microprobe analysis is essential to an understanding of the processes by which such magnetite formed.

We used high-resolution STEM (15, 16) to characterize and determine the origin of the iron oxides in basalt from the sheeted dike complex in DSDP hole 504B, located in crust that is 5.9 million years old and  $\sim 200$  km south of the Costa Rica rift. The sample, chosen as representative of a large number studied by other methods, is a massive basalt (sample 107-1; 87 to 90 cm) recovered from the upper part (depth of 870 m within the igneous basement) of the sheeted dike com-

plex during DSDP leg 83. The primary minerals in this basalt have been subjected to hydrothermal alteration that is equivalent to greenschist facies metamorphism (17, 18).

The primary opaque mineral is subhedral to euhedral titanomagnetite that is typically a few hundred micrometers in diameter (Fig. 1). Some titanomagnetite appears to be homogeneous in SEM backscattered electron (BSE) images and in reflected light. Electron microprobe analyses of apparently unaltered parts of titanomagnetite grains give compositions ranging from  $Usp_{61}$  to  $Usp_{74}$ . Some parts of titanomagnetite grains have a mottled texture and are composed of intergrown micrometer-sized sphene and titanomagnetite (Fig. 1). Other areas appear to be homogeneous titanomagnetite, as observed from BSE images, but contain minor Si and Ca, indicative of sphene. In the latter, extremely fine lamellae  $\sim 400$  Å in width are oriented in two directions nearly perpendicular to each oth-

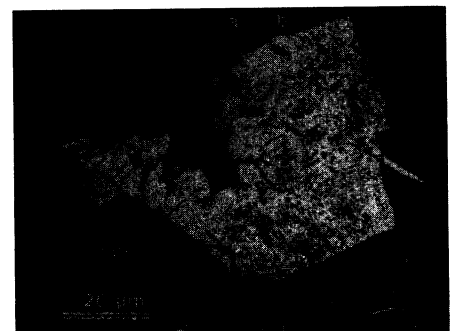


**Fig. 1.** Backscattered electron image of a subhedral titanomagnetite grain (white) showing partial alteration to sphene (gray, mottled texture). The image was taken from an ion-milled specimen prepared for STEM observation. The areas marked a and b are shown in STEM images in Figs. 2 and 3, respectively. Abbreviations: Ch, chlorite; Cpx, clinopyroxene; Sph, sphene; and Tmt, titanomagnetite that appears to be unaltered.

Department of Geological Sciences, University of Michigan, Ann Arbor, MI 48109.

\*Present address: Department of Marine Resources, National Sun Yat-sen University, Kaohsiung 80424, Taiwan, Republic of China.